

On the Ideal Number of Groups for Isometric Gradient Propagation

Bum Jun Kim¹Hyeyeon Choi¹Hyeonah Jang¹Sang Woo Kim¹¹Department of Electrical Engineering., Pohang University of Science and Technology, Pohang, South Korea

Abstract

Recently, various normalization layers have been proposed to stabilize the training of deep neural networks. Among them, group normalization is a generalization of layer normalization and instance normalization by allowing a degree of freedom in the number of groups it uses. However, to determine the optimal number of groups, trial-and-error-based hyperparameter tuning is required, and such experiments are time-consuming. In this study, we discuss a reasonable method for setting the number of groups. First, we find that the number of groups influences the gradient behavior of the group normalization layer. Based on this observation, we derive the ideal number of groups, which calibrates the gradient scale to facilitate gradient descent optimization. Our proposed number of groups is theoretically grounded, architecture-aware, and can provide a proper value in a layer-wise manner for all layers. The proposed method exhibited improved performance over existing methods in numerous neural network architectures, tasks, and datasets.

1 INTRODUCTION

Deep neural networks have recently shown significant performance in various fields. Despite their current success, in the past, deep neural networks were known to be difficult to train. To stabilize the training of a deep neural network, normalization layers, such as batch normalization [Ioffe and Szegedy, 2015], have been proposed. Normalization layers have addressed the difficulty in the optimization of deep neural networks and are used in most deep neural networks at present.

Other widely used normalization layers include layer normalization [Ba et al., 2016], instance normalization [Ulyanov et al., 2016], and group normalization [Wu and

He, 2020]. These behave similarly in that they apply mean and standard deviation (std) normalization and an affine transform. The difference lies in the units used for computing the mean and std. For example, for n features, layer normalization computes a single mean and std for normalization, whereas instance normalization computes n means and stds. Meanwhile, group normalization partitions n features into G groups to compute G means and stds. From this perspective, layer normalization is a special case of group normalization for $G = 1$, and instance normalization is a special case of group normalization for $G = n$. Thus, group normalization is more comprehensive and has a degree of freedom from the setting of the number of groups. When the number of groups is set to a specific value, there is a possibility of suboptimality, which leaves room for setting a more appropriate number of groups to further improve the performance.

The setting of the number of groups is also mentioned in the original paper on group normalization [Wu and He, 2020]. By experimenting with several trials with $G = 1, 2, 4, \dots$, they evaluated the ImageNet accuracy. They observed low accuracy at both extremes of $G = 1$ and $G = n$. In particular, they empirically found the highest accuracy at $G = 32$ and recommended this as the default value for the number of groups in group normalization. Accordingly, various studies using group normalization have employed $G = 32$ [Kirillov et al., 2019a, Ho et al., 2020, Zhu et al., 2021, Yang et al., 2019].

However, this approach to setting the number of groups has several problems. First, the corresponding number of groups lacks theoretical validation. This is because the claim that $G = 32$ yields the highest performance is confirmed only through empirical observations. Second, the neural network architecture is not considered. When a different architecture is employed, there is a possibility that $G = 32$ is suboptimal; therefore, hyperparameter tuning by trial and error is required again to set the optimal number of groups. For example, Dai et al. [2021] used $G = 16$, whereas Michalski et al. [2019] used $G = 4$. Furthermore, Song et al.

[2021] designed a neural network with a different number of groups for each layer. Training a deep neural network is time-consuming, and many hyperparameters already exist; employing an additional hyperparameter leads to a significantly high processing cost [Falkner et al., 2018, Yang et al., 2021, Cui and Bai, 2019]. Third, $G = 32$ is not guaranteed to be optimal for all group normalization layers in a deep neural network using tens or hundreds of layers. In other words, since the optimal number of groups can be different for each layer, the number of groups in a layer-wise manner G^l should be considered.

In this study, we propose an appropriate method for determining the number of groups. First, we theoretically analyze the effect of the number of groups on the back-propagation of group normalization. In this regard, we consider a gradient condition that facilitates the training of the neural network and derive the ideal number of groups that satisfies the gradient condition. Second, we show that the ideal number of groups we derived is affected by the width of the neural network. Hence, the ideal number of groups exhibits different values depending on the number of input and output features in the neural network architecture. Third, we demonstrate that the ideal number of groups varies for each layer. In summary, for setting the number of groups, we propose a reasonable method that is theoretically grounded, architecture-aware, and able to provide a proper value for all layers in a layer-wise manner.

For the application of the ideal number of groups, we propose the practical number of groups and apply it to several training experiments on deep neural networks. The proposed practical number of groups demonstrated higher performance in various tasks, architectures, and datasets.

2 IDEAL NUMBER OF GROUPS

2.1 THEORETICAL ANALYSIS

Notation In this paper, we use the notations $E[x_i]$ and $Var[x_i]$ to denote the mean and variance computed along the feature, i -axis. We do not use sample variance.¹

Formulation Consider a unit block that consists of a weight layer, group normalization, and ReLU activation function (Figure 1). First, we denote n_{in}^l -dimensional input features in the l -th block as $\mathbf{x}^l = (x_1^l, x_2^l, \dots, x_{n_{in}^l}^l)$. Weight in the l -th block is denoted as $W^l \in R^{n_{in}^l \times n_{out}^l}$. We

¹Some libraries apply Bessel’s correction by default when measuring the variance. To obtain correct results such as those in Table 1, it should be turned off. For example, in PyTorch, `torch.var(input, unbiased=False)` should be used to apply a biased estimator. In fact, `unbiased=False` is specified when `torch.nn.GroupNorm()` measures the standard deviation.

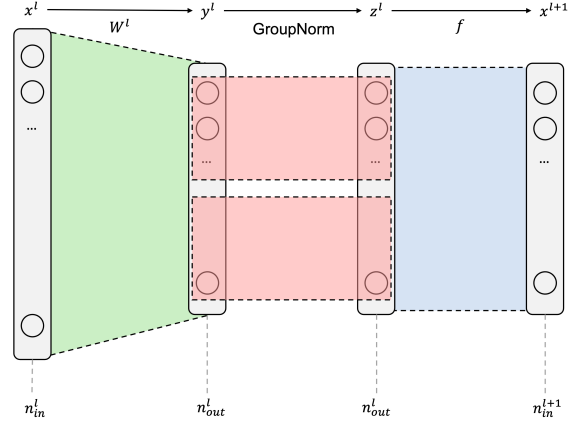


Figure 1: Illustration of the unit block.

assume zero-mean weights, as Glorot and Bengio [2010] and He et al. [2015] did. The weight layer produces output feature \mathbf{y}^l , where

$$y_j^l = \sum_{i=1}^{n_{in}^l} W_{ij}^l x_i^l. \quad (1)$$

Now, group normalization with the number of groups G^l is applied to \mathbf{y}^l to produce

$$z_{(s-1)n_g^l+j}^l = \frac{y_{(s-1)n_g^l+j}^l - \mu_s^l}{\sqrt{(\sigma_s^l)^2}}, \quad (2)$$

where

$$\mu_s^l = \frac{1}{n_g^l} \sum_{j=1}^{n_g^l} y_{(s-1)n_g^l+j}^l, \quad (3)$$

$$(\sigma_s^l)^2 = \frac{1}{n_g^l} \sum_{j=1}^{n_g^l} (y_{(s-1)n_g^l+j}^l - \mu_s^l)^2, \quad (4)$$

$$n_g^l = \frac{n_{out}^l}{G^l}, \quad (5)$$

for $s = 1, 2, \dots, G^l$. The above equations mean partitioning n_{out}^l features into G^l groups and normalizing features in each group using the corresponding mean μ_s^l and std σ_s^l . In group normalization, an affine transform of $\gamma z_k^l + \beta$ is additionally used. Following De and Smith [2020] and Zhang et al. [2019], we use the default values, *i.e.*, $\gamma = 1$ and $\beta = 0$. Finally, the activation function f results in the next feature at the $(l+1)$ -th block:

$$x_i^{l+1} = f(z_k^l). \quad (6)$$

In summary, we obtain \mathbf{x}^{l+1} from \mathbf{x}^l by passing a unit block. Here, we consider the following property of the unit block.

Definition 1 A unit block mapping \mathbf{x}^l to \mathbf{x}^{l+1} is isometric with respect to gradient propagation if

$$\text{Var} \left[\frac{\partial L}{\partial x_i^{l+1}} \right] = \text{Var} \left[\frac{\partial L}{\partial x_i^l} \right], \quad (7)$$

where L denotes a loss function.

This property ensures that the gradient scale is the same in both layers, which prevents unstable optimization due to exploding and vanishing gradients during gradient descent. For example, if the two variances are 10 and 1, this implies an imbalance in the gradient scale, which leads to an unstable optimization in the gradient descent. To stabilize the optimization, it is desirable to obtain the same or the most similar gradient scale. Note that the imbalance in the gradient scale is accumulated by passing tens or hundreds of unit blocks, which results in an exploding or vanishing gradient. So we aim to ensure that each unit block is isometric with respect to gradient propagation (Section 4). This property was also the objective of Glorot and Bengio [2010], He et al. [2015], and Klambauer et al. [2017]. In the remainder of our paper, unless specified otherwise, we use the term isometricity to discuss gradient propagation, not forward propagation.

Here, we claim that the number of groups affects the gradient variance. Our goal is to determine the solution for the number of groups that induces the isometric gradient propagation of the unit block. We investigate this, the ideal number of groups G_{ideal}^l .

Gradient propagation on weight layer First, from Eq. 1, note that an input feature x_i^l affects all output features $y_1^l, y_2^l, \dots, y_{n_{out}^l}^l$. From the chain rule for partial derivatives, we have

$$\frac{\partial L}{\partial x_i^l} = \sum_{j=1}^{n_{out}^l} \frac{\partial L}{\partial y_j^l} \frac{\partial y_j^l}{\partial x_i^l}. \quad (8)$$

By computing the variance, we see that n_{out}^l components affect the variance:

$$\text{Var} \left[\frac{\partial L}{\partial x_i^l} \right] = n_{out}^l \text{Var} [W^l] \text{Var} \left[\frac{\partial L}{\partial y_j^l} \right]. \quad (9)$$

Gradient propagation on group normalization Second, we investigate the backward propagation of group normalization. Notably, the gradients propagate only within the group. Consider the case in which a feature y_j^l belongs to the r -th group. By Eqs. 3 and 4, we have

$$\frac{\partial \mu_r^l}{\partial y_j^l} = \frac{1}{n_g^l}, \quad (10)$$

$$\frac{\partial [(\sigma_r^l)^2]}{\partial y_j^l} = \frac{2(y_j^l - \mu_r^l)}{n_g^l}. \quad (11)$$

From Eq. 2, we find that the partial derivative differs depending on whether the index matches. We consider two cases:

$$\frac{\partial z_k^l}{\partial y_j^l} = \begin{cases} \frac{1 - \frac{1}{n_g^l}(1 + (z_k^l)^2)}{\sigma_r^l}, & \text{if } k = j. \end{cases} \quad (12)$$

$$\frac{\partial z_k^l}{\partial y_j^l} = \begin{cases} -\frac{\frac{1}{n_g^l}(1 + z_k^l z_j^l)}{\sigma_r^l}, & \text{if } k \neq j. \end{cases} \quad (13)$$

From the chain rule for partial derivatives, we obtain

$$\frac{\partial L}{\partial y_j^l} = \sum_{k=1}^{n_g^l} \frac{\partial L}{\partial z_k^l} \frac{\partial z_k^l}{\partial y_j^l} \quad (14)$$

$$= T_1 - T_2 - T_3, \quad (15)$$

where

$$T_1 = \frac{1}{\sigma_r^l} \left(\frac{\partial L}{\partial z_k^l} \right), \quad (16)$$

$$T_2 = \frac{1}{\sigma_r^l} \frac{1}{n_g^l} \left(\sum_{k=1}^{n_g^l} \frac{\partial L}{\partial z_k^l} \right), \quad (17)$$

$$T_3 = \frac{1}{\sigma_r^l} \frac{1}{n_g^l} z_j^l \left(\sum_{k=1}^{n_g^l} z_k^l \frac{\partial L}{\partial z_k^l} \right). \quad (18)$$

By computing the variance, we have

$$\text{Var} [T_1] = \frac{1}{(\sigma_s^l)^2} \text{Var} \left[\frac{\partial L}{\partial z_k^l} \right], \quad (19)$$

$$\text{Var} [T_2] = \frac{1}{(\sigma_s^l)^2} \frac{1}{n_g^l} \text{Var} \left[\frac{\partial L}{\partial z_k^l} \right], \quad (20)$$

$$\text{Var} [T_3] = \frac{1}{(\sigma_s^l)^2} \frac{3}{n_g^l} \text{Var} \left[\frac{\partial L}{\partial z_k^l} \right]. \quad (21)$$

The third equation holds because $E[(z_k^l)^2 \frac{\partial L}{\partial z_k^l}] = 0$ and $E[(z_k^l)^4] = 3$ for normalized feature z_k^l . We denote the s -th group to represent an arbitrary group. The variance is computed across all features, not the features within a group. Summarizing Eqs. 19-21, we obtain

$$\text{Var} \left[\frac{\partial L}{\partial y_j^l} \right] = \frac{1}{(\sigma_s^l)^2} \left(1 + \frac{4}{n_g^l} \right) \text{Var} \left[\frac{\partial L}{\partial z_k^l} \right]. \quad (22)$$

Note that the number of groups G^l is involved in here because $n_g^l = \frac{n_{out}^l}{G^l}$. Thus, the number of groups affects the gradient propagation on the group normalization layer. We exploit this fact as a key to configure the unit block to the state that is closest to isometric.

Gradient propagation on activation function Here, we investigate the activation function. To derive the variance around the activation function, we introduce the following two properties.

Definition 2 Assume a random variable $X \sim \mathcal{N}(0, \sigma^2)$ and an arbitrary random variable Y . For a given activation function f , we define forward activation gain $F_{f,\sigma}$ and backward activation gain $B_{f,\sigma}$ as follows:

$$F_{f,\sigma} = \frac{E[(f(X))^2]}{\text{Var}[X]}, \quad (23)$$

$$B_{f,\sigma} = \frac{\text{Var}[f'(X)Y]}{\text{Var}[Y]}. \quad (24)$$

In particular, if $E[Y] = 0$, we have $B_{f,\sigma} = E[(f'(X))^2]$.

Remark 1 If $f(x) = \text{ReLU}(x) = \max(0, x)$, we have $F_{f,\sigma} = B_{f,\sigma} = \frac{1}{2}$.

Especially for ReLU, the two gains are independent of σ . However, for the other activation functions, the two gains can vary depending on σ (Section 2.3).

Now we investigate the variance around the activation function. By Eq. 6, we see that

$$\frac{\partial L}{\partial z_k^l} = \frac{\partial L}{\partial x_i^{l+1}} \frac{\partial x_i^{l+1}}{\partial z_k^l} = \frac{\partial L}{\partial x_i^{l+1}} f'(z_k^l). \quad (25)$$

Thus,

$$\text{Var} \left[\frac{\partial L}{\partial z_k^l} \right] = B_{f,\sigma} \text{Var} \left[\frac{\partial L}{\partial x_i^{l+1}} \right]. \quad (26)$$

In addition, investigating the forward propagation of the $(l-1)$ -th block,

$$(\sigma_s^l)^2 = \text{Var} [y_j^l] = n_{in}^l \text{Var} [W^l f(z_i^{l-1})] \quad (27)$$

$$= n_{in}^l E[(W^l)^2] E[(f(z_i^{l-1}))^2] \quad (28)$$

$$= n_{in}^l F_{f,\sigma} \text{Var} [W^l]. \quad (29)$$

Gradient propagation on unit block Finally, from Eqs. 9, 22, and 26, we obtain the gradient equation from \mathbf{x}^l to \mathbf{x}^{l+1} :

$$\text{Var} \left[\frac{\partial L}{\partial x_i^l} \right] = \frac{n_{out}^l}{n_{in}^l} \left(1 + \frac{4}{n_g^l} \right) \text{Var} \left[\frac{\partial L}{\partial x_i^{l+1}} \right]. \quad (30)$$

Let $K(G^l)$ be the ratio of two variances as

$$K(G^l) = \frac{n_{out}^l}{n_{in}^l} \left(1 + \frac{4}{n_g^l} \right) = \frac{n_{out}^l + 4G^l}{n_{in}^l}. \quad (31)$$

Algorithm 1 Compute $G_{practical}^l$

Require: n_{in}^l and n_{out}^l .

- 1: Compute the ideal number of groups:
 $G_{ideal}^l = (n_{in}^l - n_{out}^l)/4$.
 - 2: Apply lower bound: $G^l = \max(1, G_{ideal}^l)$.
 - 3: Apply upper bound: $G^l = \min(G^l, n_{out}^l)$.
 - 4: Compute the log of the number of groups: $\log_2 G^l$.
 - 5: Obtain divisor set of n_{out}^l as $[n_{out}^l]$.
 - 6: Compute log of set $[n_{out}^l]$ as $\log_2 [n_{out}^l]$.
 - 7: Find the closest value of $\log_2 G^l$ from the set $\log_2 [n_{out}^l]$ as l_g .
 - 8: Compute the practical number of groups:
 $G_{practical}^l = 2^{l_g}$.
 - 9: **return** $G_{practical}^l$.
-

When $K(G^l) = 1$, the unit block is isometric with respect to gradient propagation. Thus, our goal is to find the number of groups G^l that satisfies $K(G^l) = 1$. Ideally, this condition can be satisfied if the group normalization has

$$G_{ideal}^l = \frac{n_{in}^l - n_{out}^l}{4}, \quad (32)$$

which we call the ideal number of groups. Interestingly, the ideal number of groups depends on the architecture of the neural network, especially the number of input and output features of the weight layer. For example, for an l -th unit block with 128 input features and 64 output features, applying $G^l = 16$ provides isometricity of the unit block. The use of this formula allows us to set an appropriate number of groups on a given layer or architecture without any tuning experiments. Intuitively, it is desirable to have a different number of groups depending on each width. In other words, it is unnatural to apply $G^l = 32$ to all layers, regardless of the variety of width of the deep neural network.

However, the ideal number of groups may not be applicable in a practical scenario depending on n_{in}^l and n_{out}^l . For example, if $n_{in}^l = n_{out}^l = 128$, then $G_{ideal}^l = 0$, which cannot be employed in group normalization. Note that group normalization is applied to n_{out}^l features. Thus, 1) the number of groups should have lower and upper bounds of $1 \leq G_{ideal}^l \leq n_{out}^l$, and 2) n_{out}^l should be divisible by an integer G_{ideal}^l . Considering this, we seek a practical number of groups.

Definition 3 Let $[n_{out}^l]$ be the divisor set of n_{out}^l . Find $G^l \in [n_{out}^l]$ where $K(G^l)$ is closest to 1. We refer to the result as the practical number of groups $G_{practical}^l$.

The objective of finding the practical number of groups is to configure the unit block to the state that is closest to isometric, facilitating gradient descent optimization. We consider three cases:

Table 1: Empirical validation of Eqs. A to D. The results were in agreement with the theoretical expectations.

$(n_{in}^l, n_{out}^l, G^l)$	Eq. A		Eq. B		Eq. C		Eq. D	
	Empirical	Theoretical	Empirical	Theoretical	Empirical	Theoretical	Empirical	Theoretical
(1024, 512, 128)	511.236	512	1.979	2	0.500	0.5	0.995	1
(512, 256, 64)	255.160	256	1.959	2	0.499	0.5	0.989	1
(256, 128, 32)	127.189	128	2.015	2	0.500	0.5	1.032	1
(128, 64, 16)	63.185	64	1.900	2	0.500	0.5	0.992	1

Case 1. If $n_{in}^l \leq n_{out}^l$, then $K(G^l)$ is always greater than one. Thus we seek G^l that yields the smallest $K(G^l)$. Because $K(G^l)$ increases linearly with G^l , we choose the smallest G^l , i.e., $G_{practical}^l = 1$. In fact, this is equivalent to applying a lower bound to the ideal number of groups.

Case 2. If $n_{in}^l \geq 5n_{out}^l$, we have $K(G^l) = (n_{out}^l + 4G^l)/n_{in}^l \leq 1$. We need to find G^l that results in the highest $K(G^l)$. Thus, we choose $G_{practical}^l = n_{out}^l$. Similarly, this is equivalent to applying an upper bound to the ideal number of groups.

Case 3. If $n_{out}^l < n_{in}^l < 5n_{out}^l$, then we choose the number of groups in the divisor set $[n_{out}^l]$ that is closest to the ideal number of groups.

From the above analyses, we conclude with the following theorem.

Theorem 1 *Algorithm 1 yields the practical number of groups $G_{practical}^l$.*

For example, if $n_{in}^l = n_{out}^l = 128$, by Case 1, we choose $G_{practical}^l = 1$. In this scenario, because $K(G^l) = 1 + 4G^l/128$, we obtain $K(1) = 1.03125$. However, choosing a different number of groups such as 32 results in $K(32) = 2$, which results in an imbalance in the gradient scale.

2.2 EMPIRICAL VALIDATION

In this section, we test the validity of our derivation. We target Eqs. 9, 22, 26, and 30, which are our main results. The four equations are rewritten as follows:

$$Var \left[\frac{\partial L}{\partial x_i^l} \right] / Var \left[\frac{\partial L}{\partial y_j^l} \right] = n_{out}^l Var [W^l], \quad (A)$$

$$(\sigma_s^l)^2 Var \left[\frac{\partial L}{\partial y_j^l} \right] / Var \left[\frac{\partial L}{\partial z_k^l} \right] = 1 + \frac{4}{n_g^l}, \quad (B)$$

$$Var \left[\frac{\partial L}{\partial z_k^l} \right] / Var \left[\frac{\partial L}{\partial x_i^{l+1}} \right] = B_{f,\sigma}, \quad (C)$$

$$Var \left[\frac{\partial L}{\partial x_i^l} \right] / Var \left[\frac{\partial L}{\partial x_i^{l+1}} \right] = \frac{n_{out}^l}{n_{in}^l} \left(1 + \frac{4}{n_g^l} \right). \quad (D)$$

First, we empirically measure the left-hand side of Eqs. A to

D (Empirical) and compare the results with the right-hand side (Theoretical). We use two unit blocks, where $W^1 \in R^{n_{in} \times n_{in}}$, and $W^2 \in R^{n_{in} \times n_{out}}$ with unit variance. We generate artificial random data sampled from the standard normal distribution. The random data are provided to the first unit block, and we measure the ratios of variances targeting the second unit block. The loss function L can be defined as an arbitrary function, and we simply define it as an aggregation of the output features of the second unit block. Four cases of $(n_{in}^l, n_{out}^l, G^l)$ are tested. Considering randomness, for all results, we provide an average over 10^5 experiments.

The results are summarized in Table 1. We observed that the empirical ratio of variances matched well with theoretical expectations.

2.3 OTHER ACTIVATION FUNCTIONS

In this section, we investigate whether the ideal number of groups is applicable for other activation functions. First, consider $PReLU(x) = \max(0, x) + a \min(0, x)$ with scalar a , which is a generalization of ReLU and LeakyReLU [He et al., 2015, Maas et al., 2013]. We know that

$$E[(f(X))^2] = \int_{-\infty}^{\infty} (f(x))^2 p(x) dx \quad (33)$$

$$= \int_{-\infty}^0 (ax)^2 p(x) dx + \int_0^{\infty} x^2 p(x) dx \quad (34)$$

$$= \frac{1+a^2}{2} E[X^2], \quad (35)$$

where $p(x)$ denotes the probability density function of X . Similarly, $E[(f'(X))^2] = \frac{1+a^2}{2}$. Thus, PReLU has $F_{f,\sigma} = B_{f,\sigma} = \frac{1+a^2}{2}$. Remark 1 in Section 2.1 can be explained by $a = 0$. Moreover, the PReLU family guarantees consistent gain.

Remark 2 *The forward and backward activation gains do not vary by σ if and only if the activation function f is homogeneous $f(kx) = kf(x)$, or $f(kx) = -kf(x)$ for a scalar $k \neq 0$.*

See the Appendix for a detailed proof. For example,

Table 2: Empirical values for the forward and backward activation gains. For PReLU, slope $a = 0.25$ was used. The six activation functions on the left consistently yielded $B_{f,\sigma}/F_{f,\sigma} \approx 1$, while the five activation functions on the right did not.

Measurement	ReLU	PReLU	GELU	SiLU	ELU	SELU	Sigmoid	Tanh	Softplus	Softsign	LogSigmoid
$F_{f,0.1}$	0.500	0.531	0.255	0.252	0.928	1.876	25.079	0.981	48.438	0.751	48.495
$B_{f,0.1}$	0.500	0.531	0.256	0.253	0.929	1.879	0.062	0.981	0.251	0.757	0.251
$B_{f,0.1}/F_{f,0.1}$	1.000	1.000	1.006	1.002	1.001	1.001	0.002	1.000	0.005	1.007	0.005
$F_{f,1}$	0.500	0.532	0.425	0.356	0.645	1.000	0.293	0.394	0.921	0.183	0.921
$B_{f,1}$	0.500	0.532	0.456	0.379	0.668	1.071	0.045	0.464	0.293	0.228	0.293
$B_{f,1}/F_{f,1}$	1.000	1.000	1.072	1.067	1.036	1.072	0.153	1.178	0.318	1.245	0.319
$F_{f,10}$	0.500	0.531	0.500	0.499	0.504	0.565	0.005	0.009	0.501	0.007	0.501
$B_{f,10}$	0.500	0.531	0.506	0.507	0.520	0.613	0.007	0.053	0.461	0.026	0.461
$B_{f,10}/F_{f,10}$	1.000	1.000	1.011	1.017	1.032	1.085	1.434	5.780	0.920	3.908	0.921

Table 3: Test error (%) for MNIST classification. Lower is better. * indicates the practical number of groups.

G^1	1	2	4	8	16	32	64*	128	256	512
Error	1.827	1.720	1.773	1.730	1.727	1.720	1.670	1.753	3.240	88.650

$\text{ReLU}(x)$ and its mirror $-\text{ReLU}(x)$ share two gains that are independent of σ .

Remark 2 implies that the forward and backward gains vary by σ for other activation functions, such as SiLU and ELU [Ramachandran et al., 2018, Elfwing et al., 2018, Clevert et al., 2016]. Furthermore, their nonlinear exponential terms make it difficult to compute the exact solution of the forward and backward activation gains.

Alternatively, we provide empirical values for these two gains. We generate 10^7 samples of $X \sim \mathcal{N}(0, \sigma^2)$ and measure the forward and backward activation gains on well-known activation functions [Hendrycks and Gimpel, 2016, Klambauer et al., 2017, Zheng et al., 2015, Elliott, 1993]. Here, we list the results for σ of $\{0.1, 1, 10\}$ with various activation functions (Table 2).

Note that $\frac{B_{f,\sigma}}{F_{f,\sigma}} = 1$ is used in Eq. 30 assuming ReLU. Some activation functions, such as ReLU, PReLU, GELU, SiLU, ELU, and SELU, yielded a value near 1; thus, the practical number of groups can be safely used with these activation functions. However, $\frac{B_{f,\sigma}}{F_{f,\sigma}}$ from other activation functions, such as Sigmoid, Tanh, Softplus, Softsign, and LogSigmoid, were far from 1. If we consider this, for an arbitrary activation function, the ideal number of groups should be $G_{ideal}^l = (\frac{F_{f,1}}{B_{f,1}} n_{in}^l - n_{out}^l)/4$. See the Appendix for more results and discussions.

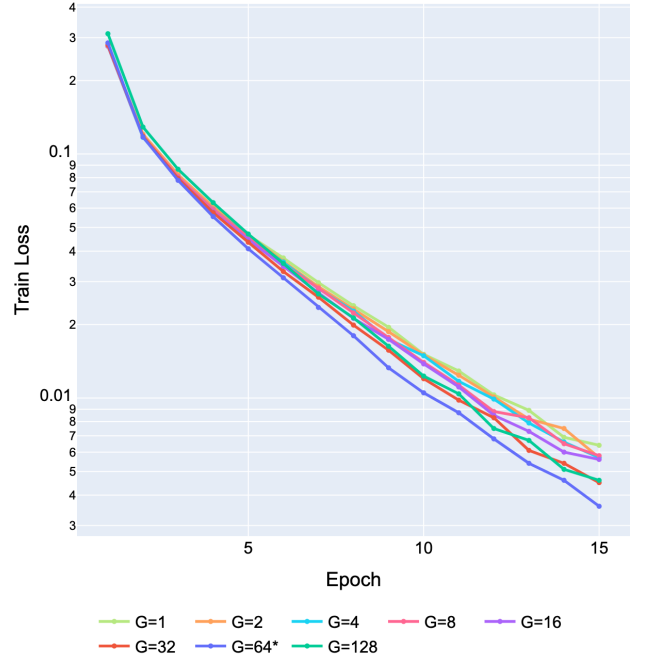


Figure 2: The learning curve of MLP for each number of groups.

3 EXPERIMENTS

3.1 IMAGE CLASSIFICATION WITH MLP

In this section, we aim to observe the performance differences of neural networks with different settings for the number of groups. We start with a simple task and then

Table 4: Test error (%) for image classification. “R” represents ResNet. Lower is better.

Setup	Oxford-IIIT Pet		Caltech-101	
	R-50	R-101	R-50	R-101
$G^l = 32$	22.894	24.067	24.021	22.781
$G^l = 1$	33.514	34.567	24.167	26.647
$G^l = G^l_{practical}$	21.119	22.924	22.368	22.247

proceed to other large-scale tasks. First, we trained multi-layer perceptrons (MLPs) for MNIST image classification. The simplicity of this task allows us to experiment with extensive numbers of groups. We used a two-layer MLP of 512 hidden nodes with group normalization and ReLU. Because $n^1_{in} = 784$ for MNIST data and $n^1_{out} = 512$, we have $G^1_{ideal} = 68$ and thus $G^1_{practical} = 64$.

An average over three runs is reported for each result (Table 3). The highest accuracy was found in $G^1 = 64$, which corresponds to $G^1_{practical}$. Others, such as $G^1 = 32$ and $G^1 = 1$, worked fine but they left with possible improvements. Figure 2 shows the learning curve of MLP for each number of groups. Because other conditions are the same, we can see that choosing the number of groups affected the learning curve of train loss, where $G^l = 64$ yielded faster convergence compared to others. We conclude that the improved accuracy came from the improved optimization achieved by choosing $G^l = 64$.

3.2 IMAGE CLASSIFICATION WITH RESNET

Second, we conducted experiments on convolutional neural networks (CNNs) for image classification. We targeted ResNet [He et al., 2016], which is a standard model used for image classification. After replacing the existing batch normalization layers with group normalization, we compared the performance with different numbers of groups. Because ResNet uses tens or hundreds of layers and is computationally expensive to train, we compared performance from three settings of the number of groups: $G^l = 32$ as the default value of group normalization, $G^l = 1$ corresponding to layer normalization, and $G^l = G^l_{practical}$ we proposed.

We targeted two datasets: Oxford-IIIT Pet and Caltech-101 [Parkhi et al., 2012, Fei-Fei et al., 2007]. The Oxford-IIIT Pet dataset includes 7K pet images of 37 classes, and the Caltech-101 dataset includes 9K object images of 101 classes with a background category. See the Appendix for details on experiments, such as the used hyperparameters. An average over three runs is reported for each result (Table 4).

We observed that when $G^l = G^l_{practical}$ was employed, it achieved a higher accuracy than when $G^l = 32$ or $G^l = 1$. The performance improvement was consistently confirmed

Table 5: Panoptic segmentation results, where a higher number is better.

Setup	PQ	PQ th	PQ st
$G^l = 32$	41.750	49.357	30.268
$G^l = 1$	41.461	49.688	29.043
$G^l = G^l_{practical}$	42.147	49.816	30.572

Table 6: Object detection results for Faster R-CNN GN+WS, where a higher number is better.

Setup	AP	AP ⁵⁰	AP ⁷⁵
$G^l = 32$	40.5	61.0	44.2
$G^l = 1$	40.4	60.9	44.3
$G^l = G^l_{practical}$	40.7	61.2	44.6

in the two datasets and ResNet-{50, 101}.

3.3 PANOPTIC SEGMENTATION WITH PFPN

Panoptic segmentation is a task that simultaneously solves semantic and instance segmentation [Kirillov et al., 2019b]. In other words, panoptic segmentation performs both pixel-wise classification and instance delineation. It is a large-scale downstream task that uses a CNN. Here, we focus on the panoptic feature pyramid network (PFPN), one of the representative models employed in the panoptic segmentation task [Kirillov et al., 2019a]. In addition, the PFPN originally exploited group normalization with $G^l = 32$. We compare the performance of the PFPN for $G^l = 32$, $G^l = 1$, and $G^l = G^l_{practical}$.

The COCO-panoptic dataset [Lin et al., 2014], which includes labeled 80 things and 53 stuff, was used for training and testing. We measured the panoptic quality (PQ), a commonly used performance index for the task [Kirillov et al., 2019b], and its variants PQth and PQst for thing and stuff, respectively (Table 5). The use of $G^l = G^l_{practical}$ resulted in a higher PQ than with $G^l = 32$ or $G^l = 1$. In particular, in the three indices, neither $G^l = 32$ nor $G^l = 1$ showed a clearly superior result, but for $G^l = G^l_{practical}$, higher PQ was consistently observed in all three indices.

3.4 OBJECT DETECTION WITH FASTER R-CNN GN+WS

Qiao et al. [2019] suggested that when group normalization is used, improved training is possible when weight standardization is applied. They experimented with a combination of group normalization and weight standardization for various tasks. Motivated by this practice, we tested the application of the practical number of groups for the case of using group normalization and weight standardization.

The target model was Faster R-CNN with group normalization and weight standardization (GN+WS), which is an improved variant of Faster R-CNN, where the existing batch normalization layers are replaced with group normalization, and weight standardization is applied in the convolution layers [Ren et al., 2017, Qiao et al., 2019]. The target task was object detection, which is a representative downstream task using a CNN. For training and testing, we used the COCO 2017 dataset, which consists of 118K training images, 5K validation images, and 41K test images. Average precision (AP), which is a commonly used index, and its variants (AP⁵⁰ and AP⁷⁵) at IoU = 50 and IoU = 75 were measured (Table 6). Applying $G^l = G_{practical}^l$ resulted in minor but consistent improvements compared to $G^l = 32$ or $G^l = 1$.

4 DISCUSSION

Glorot and Bengio [2010] discussed the condition under which the variance becomes equal for forward and backward propagation. Assuming a neural network composed of weight and sigmoid layers, for forward and backward propagation, they derived the following two conditions:

$$n_{in}^l Var[W^l] = 1, n_{out}^l Var[W^l] = 1. \quad (36)$$

However, when $n_{in}^l \neq n_{out}^l$, because both conditions cannot be simultaneously satisfied, they proposed $Var[W^l] = \frac{2}{n_{in}^l + n_{out}^l}$ as a compromise to get as close to the two conditions as possible. This is applied at the initialization of the neural network to control the weights to attain the corresponding variance. He et al. [2015] proposed another initialization method that considers the use of ReLU. These studies provide several notable points.

Perfect isometricity is not required. As mentioned above, it is difficult to equalize the variance in the forward and backward propagation simultaneously. In other words, it is difficult to obtain isometricity with respect to both forward and backward propagations. Glorot and Bengio [2010] presented a compromising alternative, and He et al. [2015] considered only forward variance. Furthermore, even if the neural network was isometric at initialization, the isometricity would vanish during training. For example, weight decay reduces the weight norm during training, which causes it to lose isometricity. In summary, the initialization method of Glorot and Bengio [2010] and He et al. [2015] helps in training by making the neural network partially isometric but does not pursue perfect isometricity.

Their assumptions differ from the architectures of practical neural networks. Glorot and Bengio [2010] assumed that a neural network comprises a combination of weight layers and sigmoid activation functions. For this sce-

nario, they derived the consecutive accumulation of backward variance from the l -th to l' -th layer as

$$Var\left[\frac{\partial L}{\partial x_i^l}\right] = Var\left[\frac{\partial L}{\partial x_i^{l'}}\right] \prod_{m=l}^{l'-1} n_{out}^m Var[W^m]. \quad (37)$$

Thus, if Eq. 36 holds for each layer, then Eq. 37 is satisfied, which makes the entire neural network isometric. Similarly, in our paper, we discussed the isometricity of a unit block composed of a weight layer, group normalization, and ReLU activation function. If a neural network is composed of only these unit blocks without any other operations, the use of an ideal number of groups will ensure isometricity for the entire neural network. However, Mishkin and Matas [2016] argued that other operations, such as the maxpool operation and other activation functions, should be considered in practice. Because it is difficult to deal with all cases theoretically, they proposed normalizing the variance after empirically measuring it in a neural network. Practical neural networks include various operations such as strided operations and skip or dense connections. When these operations are exploited in conjunction with unit blocks in a neural network, it is difficult to conclude that the isometricity of the unit block guarantees the isometricity of the entire neural network.

Despite these limitations, the initialization methods of Glorot and Bengio [2010] and He et al. [2015] have been successfully deployed in modern neural networks. The initialization method of He et al. [2015] is always specified in various libraries, including `torchvision.models`, `pytorch image models (timm)`, and `MMClassification`. Several studies have reported the effectiveness of initialization methods for stable training [He et al., 2019a, Shang et al., 2017, He et al., 2019b]. These practices imply advocacy of partial isometricity for performance gain rather than opposition due to the limitation of partial isometricity.

In summary, these two viewpoints indicate that training is stabilized even if the neural network is 1) close to an isometric state rather than in a perfect isometric state and 2) isometric only in the local unit block. Similarly, our practical number of groups 1) is different from the ideal number of groups, so it is not a perfect solution and only partially makes it as isometric as possible and 2) guarantees isometricity only for the unit block, not the entire neural network. In other words, our practical number of groups provides only partial isometricity, but it is sufficient to facilitate training.

5 CONCLUSION

In this study, we proposed a practical method for determining the number of groups for group normalization. We stated the limitations of the trial-and-error-based hyperparameter tuning approach for setting the number of groups in group normalization. In this regard, we derived the ideal

number of groups, which is advantageous for gradient descent optimization. Then we proposed the practical number of groups and applied it to various tasks, including image classification, panoptic segmentation, and object detection. We confirmed that the use of the practical number of groups provides improved performance compared to using the other settings for the number of groups.

References

- Lei Jimmy Ba, Jamie Ryan Kiros, and Geoffrey E. Hinton. Layer Normalization. *CoRR*, abs/1607.06450, 2016.
- Djork-Arné Clevert, Thomas Unterthiner, and Sepp Hochreiter. Fast and Accurate Deep Network Learning by Exponential Linear Units (ELUs). In *ICLR*, 2016.
- Hua Cui and Jie Bai. A new hyperparameters optimization method for convolutional neural networks. *Pattern Recognit. Lett.*, 2019.
- Xiyang Dai, Yinpeng Chen, Bin Xiao, Dongdong Chen, Mengchen Liu, Lu Yuan, and Lei Zhang. Dynamic head: Unifying object detection heads with attentions. In *CVPR*, 2021.
- Soham De and Samuel L. Smith. Batch Normalization Biases Residual Blocks Towards the Identity Function in Deep Networks. In *NeurIPS*, 2020.
- Stefan Elfving, Eiji Uchibe, and Kenji Doya. Sigmoid-weighted linear units for neural network function approximation in reinforcement learning. *Neural Networks*, 2018.
- David L Elliott. A better activation function for artificial neural networks. Technical report, 1993.
- Stefan Falkner, Aaron Klein, and Frank Hutter. BOHB: Robust and Efficient Hyperparameter Optimization at Scale. In *ICML*, 2018.
- Li Fei-Fei, Robert Fergus, and Pietro Perona. Learning generative visual models from few training examples: An incremental Bayesian approach tested on 101 object categories. *Comput. Vis. Image Underst.*, 2007.
- Xavier Glorot and Yoshua Bengio. Understanding the difficulty of training deep feedforward neural networks. In *AISTATS*, 2010.
- Kaiming He, Xiangyu Zhang, Shaoqing Ren, and Jian Sun. Delving Deep into Rectifiers: Surpassing Human-Level Performance on ImageNet Classification. In *ICCV*, 2015.
- Kaiming He, Xiangyu Zhang, Shaoqing Ren, and Jian Sun. Deep Residual Learning for Image Recognition. In *CVPR*, 2016.
- Kaiming He, Ross B. Girshick, and Piotr Dollár. Rethinking ImageNet Pre-Training. In *ICCV*, 2019a.
- Tong He, Zhi Zhang, Hang Zhang, Zhongyue Zhang, Junyuan Xie, and Mu Li. Bag of Tricks for Image Classification with Convolutional Neural Networks. In *CVPR*, 2019b.
- Dan Hendrycks and Kevin Gimpel. Gaussian error linear units (gelus). *arXiv preprint arXiv:1606.08415*, 2016.
- Jonathan Ho, Ajay Jain, and Pieter Abbeel. Denoising Diffusion Probabilistic Models. In *NeurIPS*, 2020.
- Sergey Ioffe and Christian Szegedy. Batch Normalization: Accelerating Deep Network Training by Reducing Internal Covariate Shift. In *ICML*, 2015.
- Alexander Kirillov, Ross B. Girshick, Kaiming He, and Piotr Dollár. Panoptic Feature Pyramid Networks. In *CVPR*, 2019a.
- Alexander Kirillov, Kaiming He, Ross B. Girshick, Carsten Rother, and Piotr Dollár. Panoptic Segmentation. In *CVPR*, 2019b.
- Günter Klambauer, Thomas Unterthiner, Andreas Mayr, and Sepp Hochreiter. Self-Normalizing Neural Networks. In *NIPS*, 2017.
- Tsung-Yi Lin, Michael Maire, Serge J. Belongie, James Hays, Pietro Perona, Deva Ramanan, Piotr Dollár, and C. Lawrence Zitnick. Microsoft COCO: Common Objects in Context. In *ECCV*, 2014.
- Andrew L Maas, Awni Y Hannun, Andrew Y Ng, et al. Rectifier nonlinearities improve neural network acoustic models. In *Proc. icml*, 2013.
- Vincent Michalski, Vikram Voleti, Samira Ebrahimi Kahou, Anthony Ortiz, Pascal Vincent, Chris Pal, and Doina Precup. An empirical study of batch normalization and group normalization in conditional computation. *CoRR*, abs/1908.00061, 2019.
- Dmytro Mishkin and Jiri Matas. All you need is a good init. In *ICLR*, 2016.
- Omkar M. Parkhi, Andrea Vedaldi, Andrew Zisserman, and C. V. Jawahar. Cats and dogs. In *CVPR*, 2012.
- Siyuan Qiao, Huiyu Wang, Chenxi Liu, Wei Shen, and Alan Yuille. Micro-batch training with batch-channel normalization and weight standardization. *arXiv preprint arXiv:1903.10520*, 2019.
- Prajit Ramachandran, Barret Zoph, and Quoc V. Le. Searching for Activation Functions. In *ICLR*, 2018.
- Shaoqing Ren, Kaiming He, Ross B. Girshick, and Jian Sun. Faster R-CNN: Towards Real-Time Object Detection with Region Proposal Networks. *IEEE Trans. Pattern Anal. Mach. Intell.*, 2017.

- Wenling Shang, Justin Chiu, and Kihyuk Sohn. Exploring Normalization in Deep Residual Networks with Concatenated Rectified Linear Units. In *AAAI*, 2017.
- Minsoo Song, Seokjae Lim, and Wonjun Kim. Monocular Depth Estimation Using Laplacian Pyramid-Based Depth Residuals. *IEEE Trans. Circuits Syst. Video Technol.*, 2021.
- Dmitry Ulyanov, Andrea Vedaldi, and Victor S. Lempitsky. Instance Normalization: The Missing Ingredient for Fast Stylization. *CoRR*, abs/1607.08022, 2016.
- Yuxin Wu and Kaiming He. Group Normalization. *Int. J. Comput. Vis.*, 2020.
- Ge Yang, Edward J. Hu, Igor Babuschkin, Szymon Sidor, Xiaodong Liu, David Farhi, Nick Ryder, Jakub Pachocki, Weizhu Chen, and Jianfeng Gao. Tuning Large Neural Networks via Zero-Shot Hyperparameter Transfer. In *NeurIPS*, 2021.
- Ze Yang, Shaohui Liu, Han Hu, Liwei Wang, and Stephen Lin. RepPoints: Point Set Representation for Object Detection. In *ICCV*, 2019.
- Guodong Zhang, Chaoqi Wang, Bowen Xu, and Roger B. Grosse. Three Mechanisms of Weight Decay Regularization. In *ICLR*, 2019.
- Hao Zheng, Zhanlei Yang, Wenju Liu, Jizhong Liang, and Yanpeng Li. Improving deep neural networks using soft-plus units. In *IJCNN*, 2015.
- Xizhou Zhu, Weijie Su, Lewei Lu, Bin Li, Xiaogang Wang, and Jifeng Dai. Deformable DETR: Deformable Transformers for End-to-End Object Detection. In *ICLR*, 2021.